Deep learning-based mapping of seasonal urban green space dynamics in Banjul, The Gambia

Bubacarr Jawla[1], Lamin Barrow[2], and Faye Jerreh Manneh[3]

[1]Department of Biosystem Engineering, Faculty of Agro-Industrial and Biosystems Technology, Universitas Brawijaya, Malang, Indonesia

[2]National Agricultural Research Institute (NARI), Brikama, West Coast Region, The Gambia.

[3]Faculty of Agriculture and Environmental Sciences, University of The Gambia, Faraba, Gambia

[*)] Correspondence author's email: bubacarrjawla@student.ub.ac.id

Citation:
Bubacarr Jawla, Lamin Barrow, and Faye Jerreh Manneh (2026). *Deep learning-based mapping of seasonal urban green space dynamics in Banjul, The Gambia*. Jurnal Sains Geografi. Vol. 04, No. 02

Article History:
Received: 22/10/2026
Revised: 09/11/2026
Accepted: 13/11/2026
Online: 27/11/2026
Published: 27/11/2026

Abstract

Reliable information on urban green spaces is limited in Greater Banjul, The Gambia, where vegetation is highly seasonal, and single-date satellite imagery can conflate phenology with land-cover change. This study tested a patch-based convolutional neural network (CNN) to map green spaces from Landsat 8 and 9 surface-reflectance imagery acquired in January, May, and November 2025 and compared it with random forest using a spatially blocked data split. Reference labels were created from spectral indices using date-specific Otsu-NDVI thresholds. Green spaces occupied 20,772 ha (49.5% of the land) in January, 20,588 ha (49.0%) in May, and 29,044 ha (68.0%) in November. A fixed threshold of 0.445 would have classified 2.9% of the land as green in May but 49.2% in November, demonstrating the seasonal bias that date-specific thresholds eliminate. Persistence analysis revealed that 18,372 ha (44.3% of the land) remained green on all three dates, 10,675 ha (25.7%) was seasonal, and 12,417 ha (29.9%) was never green. The CNN and random forest agreed approximately equally with the index-derived labels (overall accuracy 0.9990-0.9999), indicating rule reproduction rather than independent accuracy.

Keywords: Urban Green Space, deep learning, convolutional neural network, Landsat 8, NDVI persistence

Abstrak

Informasi yang dapat diandalkan mengenai ruang hijau perkotaan masih langka di Wilayah Metropolitan Banjul, Gambia, di mana vegetasi sangat dipengaruhi oleh musim, dan citra satelit yang diambil pada satu tanggal tertentu dapat mencampuradukkan fenologi dengan perubahan tutupan lahan. Penelitian ini menguji jaringan saraf konvolusional (CNN) berbasis patch untuk memetakan ruang hijau dari citra reflektansi permukaan Landsat 8 dan 9 yang diperoleh pada bulan Januari, Mei, dan November 2025, serta membandingkannya dengan metode random forest menggunakan pembagian data yang diblokir secara spasial. Label referensi dibuat dari indeks spektral menggunakan ambang batas Otsu-NDVI yang spesifik untuk setiap tanggal. Ruang hijau mencakup 20.772 ha (49,5% dari luas daratan) pada Januari, 20.588 ha (49,0%) pada Mei, dan 29.044 ha (68,0%) pada November. Ambang batas tetap sebesar 0,445 akan mengklasifikasikan 2,9% dari luas lahan sebagai hijau pada bulan Mei, tetapi 49,2% pada bulan November, yang menunjukkan adanya bias musiman yang dapat dihilangkan dengan menggunakan ambang batas khusus tanggal. Analisis persistensi menunjukkan bahwa 18.372 ha (44,3% dari luas lahan) tetap hijau pada ketiga tanggal tersebut, 10.675 ha (25,7%) bersifat musiman, dan 12.417 ha (29,9%) tidak pernah hijau. Model CNN dan random forest menunjukkan kesesuaian yang hampir sama dengan label yang diperoleh dari indeks (akurasi keseluruhan 0,9990–0,9999), yang mengindikasikan reproduksi aturan daripada akurasi independen.

Kata kunci: Ruang Hijau Perkotaan, pembelajaran mendalam, jaringan saraf konvolusional, Landsat 8/9, persistensi NDVI

Copyright: © 2022 by the authors. Submitted for possible open access publication under the terms and conditions of the Creative Commons Attribution (CC BY) license (https://creativecommons.org/licenses/by/4.0/).

1. INTRODUCTION

Urban green spaces include street trees, parks, gardens, peri-urban woodland, agricultural land, and remnant natural vegetation found within or in the vicinity of the built environment, and they provide regulating, provisioning, and cultural ecosystem services that are integral and vital to urban liveability (Semeraro et al., 2021). Documented benefits include the mitigation of urban heat (Sanampreet, 2020) improved public health outcomes (Department of Horticulture, School of Agriculture, Lovely Professional University, India et al., 2024) and potential reduction in environmental inequities in access to nature (Proutsos & Solomou, 2025). However, these benefits are increasingly under strain worldwide. The proportion of the world's population residing in cities is expected to increase from approximately 55% in 2018 to approximately 68% by 2050 (United Nations Department of Economic and Social Affairs, 2019) and land use projections suggest significant encroachments on vegetated and biodiverse land (Bayer et al., 2021). Consequently, there has been a growing global focus on understanding and tracking the extent and condition of urban green spaces, particularly in sustainable urban planning (Aram, 2024). Therefore, understanding and monitoring the extent and condition of urban green spaces has been a priority for sustainable urban planning on a global scale (Y. Wang, 2024).

These pressures are particularly high in sub-Saharan countries, where urban populations are increasing at an unprecedented rate, and expansion is expected to impact ecologically sensitive areas (Güneralp et al., 2017). Coastal cities in West Africa are particularly vulnerable, as they experience rapid and unplanned urban expansion, coupled with a lack of systematic monitoring of land use at the institutional level and high vulnerability to climate hazards (J. Nhantumbo et al., 2023). Vegetation is also very seasonal in this region. Changes in vegetation conditions are influenced by a distinct dry season and a rainy season throughout the Sudano-Sahelian belt, which results in vegetation conditions observed at one time of year being quite different from those observed at another (Zeng et al., 2023).

The Gambia illustrates these regional dynamics at the national level. It is a low-lying West African state centred on the Gambia River, with the Atlantic Ocean on its western border (Webb, 1992). The Greater Banjul area, which includes the capital city and its neighbouring municipalities, has a high concentration of the nation's population and economic activities in a relatively small coastal strip between the estuary of the river and the sea (Gijanto, 2013). The remaining vegetation, such as mangrove fringing vegetation, tree canopy, gardens, and crop areas, is subjected to high levels of development pressure (Ceesay et al., 2017). With little reliable and repeatable data available on the extent and seasonal distribution of green space in The Gambia, evidence-based planning solutions in Greater Banjul are dependent on this data. The outdated, systematic green space inventories in Greater Banjul and the complexity of field-based mapping make it difficult and expensive to repeat. Satellite remote sensing provides a more practical option; however, there are three interrelated problems in this context (García-Pardo et al., 2022). First, the green space map made from a single acquisition date is not sufficient to give an accurate idea of the state of vegetation in a seasonal dry area, as the same area could be considered vegetated or non-vegetated depending on the phenological phase (Neyns & Canters, 2022). This masks seasonal changes from actual land-cover changes. Second, the most used index thresholds (e.g., the fixed NDVI threshold of 0.4 (Tucker, 1979) do not apply from one date to another because the distribution of an NDVI landscape can vary significantly between dry and wet conditions (Huang et al., 2021). Third, Landsat data have a 30 m resolution, resulting in mixed pixels in fragmented urban areas, meaning that a decision based on the spectrum alone may be subject to confusion between sparse vegetation and bare soil and built surfaces (Ridwana et al., 2019). A need for methods that leverage spatial context is thus identified, and their usefulness in data-limited environments in West Africa has rarely been evaluated.

Yet, common methods of urban vegetation mapping are based on per-pixel classification and spectral indices. In combination with water and built-up indices, such as the Modified Normalised Difference Water Index (MNDWI) (Xu, 2006) and the Normalised Difference Built-up Index (NDBI) (Zha et al., 2003) The Normalised Difference Vegetation Index (NDVI) can be used to aid fast land cover separation, and thresholds are often derived statistically, such as by Otsu's (1979) method (Otsu, 1979). Since then, machine-learning classifiers, such as random forests, have been the standard for multispectral mapping because of their strength and modest tuning requirements (Papaiordanidis et al., 2020). These families handle each pixel; however, they cannot take advantage of the spatial structure of neighbouring pixels, which is informative in heterogeneous urban mosaics (Qian et al., 2020).

Deep learning and convolutional neural networks (CNNs) solve this problem by directly learning "spectral–spatial" features from the image patches. In many remote-sensing applications, consistent improvements over shallow classifiers have been reported (Butt et al., 2023; Zhang & Hong, 2018) and CNN-based land-cover labelling has been proven on a large scale (Carranza-García et al., 2019). Nonetheless, three limitations temper the interpretation of this study. First, much of the evidence comes from high-resolution imagery or study areas in Europe, North America, and East Asia, whereas moderate-resolution, freely available Landsat data, which support long-term monitoring in resource-limited environments (Wulder et al., 2019, 2022) have been relatively underused for deep learning in African cities. Second, the accuracy of reported results is often over-optimistic because the training and test sets are typically spatially correlated, so that the results overestimate the generalisation from training to testing (Ploton et al., 2020). Third, training labels are sometimes automatically generated, as in the case of spectral-index rules, which causes label noise and can make a network learn the rules used to create its reference, which can be detrimental (Algan & Ulusoy, 2020). The accuracy assessment literature for remote sensing (Castilla, 2016; Waldner, 2020) suggests an independent probability-based reference sample because the accuracy of the remote sensing data does not necessarily match the accuracy of the labels.

Studies on vegetation seasonality in drylands have also revealed that phenological variation is a first-order control on vegetation indices (Han et al., 2020; Wei et al., 2024), which has not been quantified in urban green space mapping studies or distinguished between green spaces that are all-season green and vegetation that is only transiently green. Multi-temporal NDVI analysis has also been demonstrated to be effective for characterising vegetation dynamics and recovery following environmental disturbance (Jawla, et al., 2026).

Accordingly, the literature reveals several gaps relevant to the Greater Banjul. First, there is little evidence on the use of CNN-based classification of Landsat surface-reflectance imagery for urban green-space mapping in The Gambia or comparable Sahelian coastal cities. Second, few studies combine multi-season imagery with date-specific thresholds to separate persistent from seasonal green spaces, although this distinction is essential for planning in strongly seasonal climates. Third, direct comparisons between CNN and Random Forest classifiers under spatially blocked evaluation are limited; therefore, it remains unclear whether spatial context learning yields practical advantages over a strong conventional baseline at 30 m resolution. Fourth, the dependence of reported accuracy on the label-generation strategy is seldom made explicit, which limits the credibility of the reported performance and reproducibility of the results.

This study aimed to evaluate the effectiveness of a deep-learning approach for mapping urban green spaces in Greater Banjul using Landsat 8 and 9 multispectral imagery acquired in the early dry season (January), late dry season (May), and post-rainy period (November) of 2025. The specific objectives were as follows: (i) to develop a patch-based CNN for land-cover classification (water, green space, and built-up and bare land) from six-band Landsat Collection 2 Level-2 surface-reflectance data, (ii) to map and quantify the extent of green space on each

date and to determine the persistence of green space across the three dates, (iii) to assess classification performance using Overall Accuracy, Precision, Recall, F1-score, and the Kappa coefficient under a spatially blocked data split, and to benchmark the CNN against a Random Forest classifier, and (iv) to examine the suitability and limitations of Landsat imagery and deep learning for green-space monitoring in rapidly urbanizing, seasonally dry coastal environments.

This study advances the field at the methodological, empirical, and applied levels. (i) It couples a patch-based CNN with date-specific, Otsu-derived reference thresholds so that class definitions adapt to the phenological state and quantifies, through a fixed-threshold comparison, the seasonal bias that this avoids; (ii) separates agreement with index-derived labels from accuracy measured against an independent, stratified, and visually interpreted sample; (iii) explicitly reports agreement with index-derived labels as rule reproduction rather than independent accuracy, providing a transparent evaluation protocol for weakly supervised land-cover mapping. To the authors' knowledge, this is the first multi-seasonal, deep-learning-based quantification of green space for Greater Banjul and introduces a persistence analysis that distinguishes green space that remains vegetated across seasons from vegetation that is only transiently green, a distinction single-date maps cannot recover. In applied terms, the workflow relies solely on freely available Landsat data and standard open-source tools, so it can be repeated by municipal and national agencies with limited resources. Its outputs offer a baseline for monitoring progress towards universal access to green and public spaces under Sustainable Development Goal 11.7 and for prioritising the conservation of stable green spaces (Blečić & Saiu, 2021). Because the approach is not specific to The Gambia, it is also transferable to other seasonally dry coastal cities in West Africa that face similar data constraints.

2. METHOD

The methodological workflow (**Figure 1**) involved the following steps: (i) acquisition and pre-processing of Landsat surface-reflectance imagery for the three dates used in 2025; (ii) label generation for the three dates using spectral indices; (iii) training of the patch-based CNN and a Random Forest benchmark using the dates and spatially blocked data partition; (iv) mapping of the three dates, area quantification, and analysis of green-space persistence and seasonal sensitivity; and (v) accuracy assessment as agreement with the index-derived reference labels on spatially held-out test blocks.

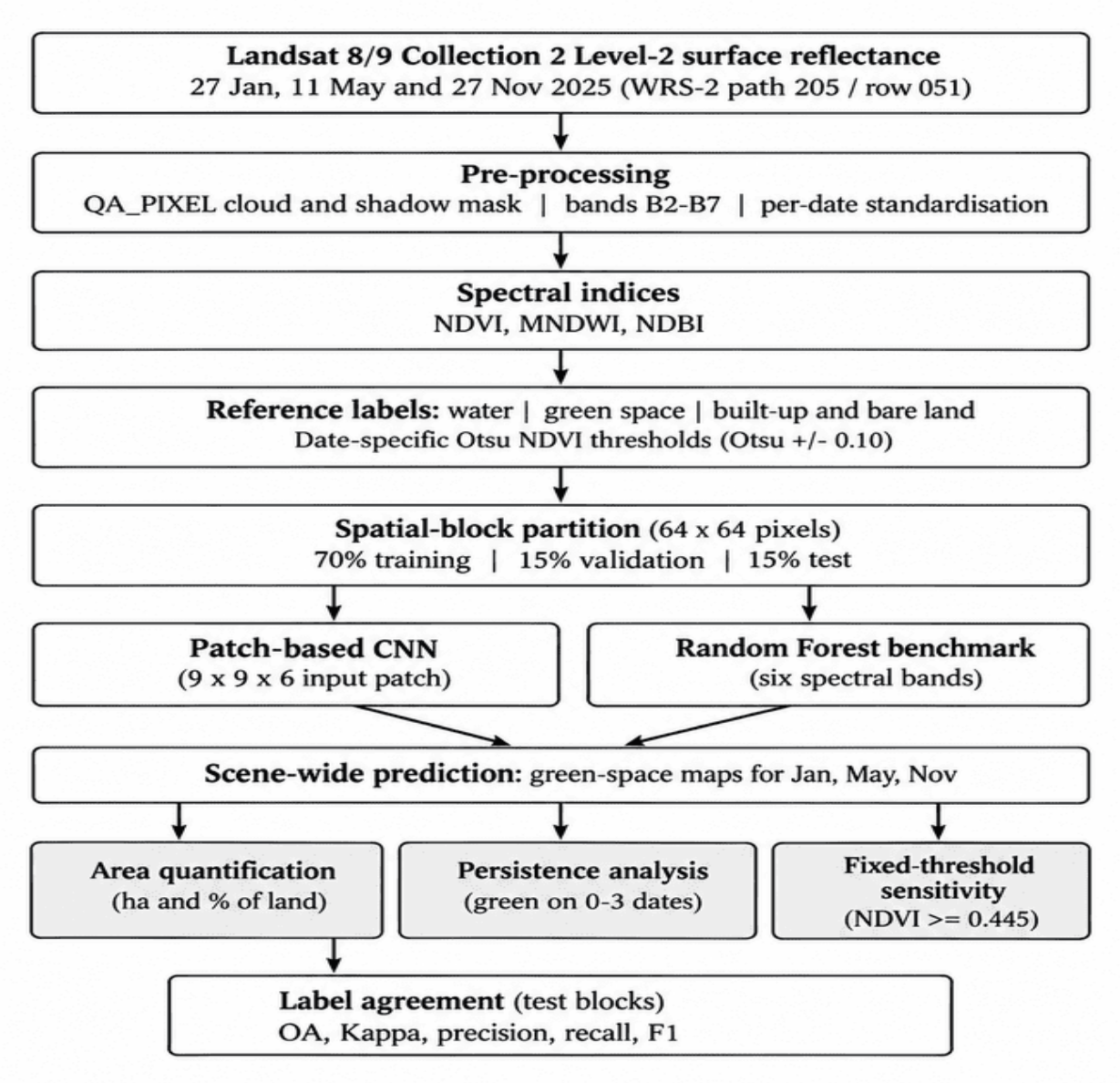


Figure 1: Methodological workflow of the study

2.1 Study Area

The study area was the Greater Banjul Peninsula on the Atlantic coast of The Gambia, with a central point at approximately 13.4°N, 16.6°W (**Figure 2**). The analysis window was 1271 × 1098 pixels at 30 m resolution (approximately 38.1 km × 32.9 km or approximately 125,600 ha), which contained the capital city and adjacent municipalities and the estuary of the Gambia River and adjacent Atlantic waters. The analysis extent was the Greater Banjul Area (GBA), which included Banjul City and Kanifing Municipality, as well as some parts of Kombo North and Kombo Central districts. The analysis window was a fixed rectangular extent of the raster that matched the Landsat WRS-2 path 205 and row 051, and included the urban area, the surrounding land, the estuary of the Gambia River, and the adjacent Atlantic waters. It comprised 1,271 × 1,098 pixels at 30 m resolution (approximately 38.1 × 32.9 km). About 65% of the window is open water, and the land area valid on the three dates is about 41,500 ha. The climate is tropical Sudano-Sahelian, with only one rainy season and a long dry season, resulting in a large seasonal variation in vegetation conditions from dry to rainy seasons.

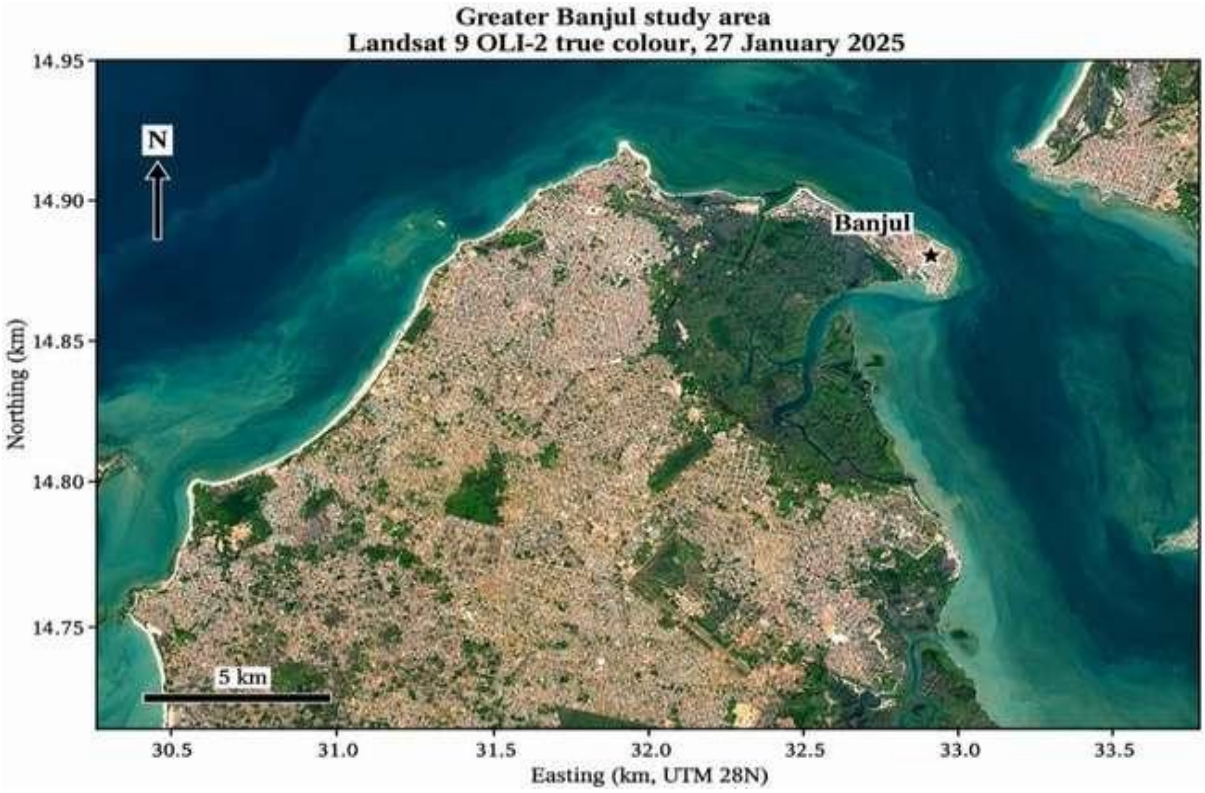


Figure 2. Study area: Greater Banjul, The Gambia, shown in a Landsat 9 OLI-2 true-colour composite of 27 January 2025 (UTM zone 28N).

2.2 Satellite data and pre-processing

Three cloud-screened "representative" Landsat Collection 2 surface-reflectance scenes were chosen to represent the three seasons – early dry (January), late dry (before the rains start, May), and immediately after the rainy season (November) – for WRS-2 path 205, row 051. The selection of scenes was based on cloud cover (CC), following the Landsat image-selection method used by Jawla et al. (2026), which required CC to be below 10% over the study area. The January, May, and November scenes also fall within the cloud-free dry season or just after the rains, when atmospheric transmissivity in The Gambia is high and stable, whereas cloud attenuation is strongest in the July–September monsoon core (Jawla et al., 2026). The areas were also selected to provide full spatial coverage of the Greater Banjul study area. The January and November images were captured using the Landsat 9 (OLI-2) instrument, and the May image was captured using Landsat 8 (OLI). The acquisition dates and sensors of the selected scenes are listed in **Table 1.**

Table 1. Landsat scenes used in the study.

Acquisition date	Sensor	Seasonal context	Path/Row
27 January 2025	Landsat 9 OLI-2	Early dry season	205/051
11 May 2025	Landsat 8 OLI	Late dry season (pre-rainy)	205/051
27 November 2025	Landsat 9 OLI-2	Post-rainy period	205/051

Bands used on every date: B2 (blue), B3 (green), B4 (red), B5 (NIR), B6 (SWIR 1), B7 (SWIR 2), and QA_PIXEL (quality mask).

Clouds for that date were masked and excluded from all analyses for that date, as per the cloud screening logic of Foga et al. (2017) for pixels flagged as fill, dilated cloud, cirrus,

cloud, or cloud shadow. Before calculating any spectral indices, the six reflective bands were converted to surface reflectance by adjusting the Collection 2 scale factor (SR = DN × 0.0000275 − 0.2) of the Landsat Collection 2 Level-2 digital numbers. The scaled surface reflectance values were used to calculate NDVI and other derived indices. The spectral bands were then band-normalised for each acquisition date using the band means and standard deviations derived from the training blocks only. The training-derived statistics were unaffected in the validation and prediction areas, thus avoiding the influence of information derived from the validation or prediction areas on the input standardisation.

2.3 Spectral indices and reference labels

Three spectral indices were calculated for each date (Equations 1–3) and used to generate reference labels: the normalised difference vegetation index (NDVI) (Pozhar, 2025), modified normalised difference water index (MNDWI) (K. Harsha & D. Gowri, 2022) and normalised difference built-up index (NDBI) (Ngandam Mfondoum et al., 2020). The surface reflectance in the near-infrared (NIR, B5), red (B4), green (B3), and shortwave infrared 1 (SWIR1, B6) bands is represented by ρ (Ji et al., 2011).

$$NDVI = (\rho_{NIR} - \rho_{Red}) / (\rho_{NIR} + \rho_{Red}) \quad (1)$$

$$MNDWI = (\rho Green - \rho SWIR1) / (\rho Green + \rho SWIR1) \quad (2)$$

$$NDBI = (\rho SWIR1 - \rho NIR) / (\rho SWIR1 + \rho NIR) \quad (3)$$

The areas were classified into three categories: water, green space, and non-vegetated land (built-up and bare land). Using MNDWI and NDBI, land was separated from water, with land defined as pixels with MNDWI < -0.05 and NDBI > -0.2. The land mask was used to separate vegetation from non-vegetated surfaces within the land mask based on the NDVI thresholds computed individually for each acquisition date. The Otsu (1979) threshold was calculated for each date based on the NDVI histogram of the land pixels (Khalil et al., 2024). Pixels used for green space were those with NDVI values at or above the Otsu threshold + 0.10, while pixels with NDVI values at or below the Otsu threshold -0.10 were classified as built-up and bare land (**Table 2)**. Pixels with NDVI values within this range were removed from the labelled set and were not classified as either of the two land cover classes during the CNN training. The ±0.10 margin therefore acted as a "guard band" that eliminated spectrally ambiguous pixels from the training labels and minimised label noise in the vicinity of the class boundary (Li et al., 2016).

Table 2. Date-specific NDVI thresholds used to generate reference labels.

Date	Otsu NDVI (land)	Green space (Otsu + 0.10)	Non-vegetated (Otsu − 0.10)
January 2025	0.345	0.445	0.245
May 2025	0.274	0.374	0.174
November 2025	0.418	0.518	0.318

Otsu values were derived from the thresholds applied (green threshold − 0.10).

The green-space class refers to land that is relatively vegetated on that date to account for the seasonal variation in the distribution of NDVI, but not as such to land that represents a certain percentage of canopy cover. This was discussed specifically in the persistence analysis and in the fixed-threshold comparison. The CNN was evaluated only against these index-derived labels, which is a form of weak supervision.

2.4 CNN architecture

A patch-based convolutional neural network (CNN) was developed to capture the spectral-spatial information of the neighbourhood around each target pixel. The input to the network was a 9 × 9-pixel (270 m × 270 m) patch with six standardised surface-reflectance bands, while the target output was the pseudo-label of the central pixel of the patch. The network architecture (**Table 3**) has four 3 × 3 convolutional layers with 32, 64, 64, and 64 filters, respectively. The first three convolutional layers were followed by batch normalisation (Xie et al., 2021), rectified linear unit (ReLU) activation, and dropout (Bhattad et al., 2024), with a dropout rate of 0.3. This was followed by a 1 × 1 convolutional layer with 32 units (Yao et al., 2022), and the final softmax layer, which yielded probabilities of each class for the three land cover classes.

One CNN model was trained independently for each acquisition date, using the pseudo-labelled data of that date. This date-specific modelling had the benefit of not training the network on a shared mapping for various seasons and sensor conditions, and it enabled a mapping of the spatial–spectral relationships to be learned from the imagery available for each date.

The 9 × 9-pixel patch was chosen for its spatial context of 270 m × 270 m around the central 30-m pixel, which corresponds to the neighbourhood around the selected central pixel. This size was chosen to reflect the local urban spatial structure, such as the intermingling of tree clusters and small green spaces with roads and built-up surfaces, and to minimise the number of other land-cover types that are more distant and could create further spectral variability. A formal patch-size sensitivity experiment was not conducted; therefore, the 9 × 9 patch should be regarded as a reasonable design choice rather than an optimised one, and other patch sizes may perform differently.

Table 3. Configuration of the CNN classifier and training data.

Component	Specification
Input	9 × 9-pixel patch (270 m × 270 m), six bands (B2–B7), standardised per date
Convolutional layers	Four 3 × 3 layers with 32, 64, 64 and 64 filters; batch normalisation and ReLU on the first three
Regularisation	Dropout, rate 0.3
Classification head	1 × 1 convolution (32 units), softmax output with three classes
Classes	Water, green space, built-up, and bare land
Training samples	Up to 12,000 per class (36,000 in total)
Validation samples	12,000
Testing samples	All remaining labelled pixels in test blocks
Optimiser	Adam, learning rate 0.001, reduced on plateau; early stopping on validation loss

2.5 Spatially blocked data partition and training

Randomly splitting the pixels can introduce spatial correlation between the samples in the training and test sets and overestimate the accuracy (Roberts et al., 2017). The study window was thus divided into non-overlapping blocks of 64 × 64 pixels (which equate to 1.9 km), and these were randomly allocated to training (70%), validation (15%), and test (15%) sets. **Up to** 12,000 samples per class (up to 36,000 in total) were taken from the training blocks and 12,000

samples in total from the validation blocks, and all remaining labelled pixels in the test blocks were reserved for testing. The CNN was given 9 × 9-pixel patches of input data, with the patches only taken from the same spatial partitionto avoid crossing the training, validation, or test block boundaries. To evaluate the CNN and Random Forest classifiers consistently and independently, the same spatial block partition was applied to both classifiers. The Adam optimiser (Zaznov et al., 2025) was used with an initial learning rate of 0.001 that was decreased when the validation loss levelled off, and training was stopped early based on the validation loss.

2.6 Random Forest benchmark

A Random Forest (RF) classifie (Isaac et al., 2017), widely regarded as a strong benchmark for multispectral classification (Kulkarni, 2025) was trained using the same labelled samples and spatial training, validation and test partitions as the CNN. Unlike the CNN, which used 9 × 9-pixel spatial patches, the RF used the six standardised surface-reflectance bands (B2–B7) of the central pixel as predictors; the 9 × 9 patch was not flattened and used as an RF input. The RF consisted of 500 decision trees, with two predictor variables randomly considered at each split, using the Gini impurity criterion. Trees were grown without a maximum depth restriction, with bootstrap sampling enabled. The same class labels, sampling strategy, and spatial partitions were used for both classifiers. This ensured that the comparison was conducted under identical data conditions while allowing the CNN to exploit spatial context and the RF to operate on pixel-level spectral information.

2.7 Green-space mapping, area quantification and persistence

Each trained model was applied to every unmasked pixel using a sliding 9 × 9 window to produce a land-cover map for each date, with Each trained model was applied to every unmasked pixel using a sliding 9 × 9 window, with zero-padding applied at the scene borders to allow predictions for pixels located at the edges of the study area. Class areas were calculated as pixel counts multiplied by 0.09 ha, and the green-space share was expressed as a percentage of land (green space plus built-up and bare land), excluding water and masked pixels. To separate stable from transient green space, a persistence analysis was performed on pixels classified as land and unmasked on all three dates. Each pixel was assigned to one of four classes according to the number of dates on which it was green: all three dates, two dates, one date, or never. Persistence shares are therefore expressed relative to this common land footprint and not to the date-specific land totals.

2.8 Seasonal sensitivity to a fixed NDVI threshold

To quantify the bias that a single threshold would introduce, the January green-space threshold (NDVI ≥ 0.445) was applied unchanged to all three dates over the land mask (MNDWI < −0.05 and NDBI > −0.2). The median land NDVI and the percentage of land at or above the threshold were computed for each date and contrasted with the date-specific classification.

2.9 Accuracy assessment

Agreement with the index-derived reference labels was evaluated on the held-out test blocks using the confusion matrix, Overall Accuracy (OA), the Kappa coefficient (Sasikala et al., 2017) and macro-averaged precision, recall and F1-score (Equations 4 to 6), where n11, n22 and n33 are the correctly classified samples of each class, N is the number of test samples, p_o and p_e are the observed and chance agreement, and P and R are precision and recall

averaged over the three classes. Because the labels were generated from spectral-index rules applied to the same bands, these metrics measure how faithfully each model reproduces the rules and are reported as agreement, not as independent accuracy.

$$OA = (n_{11} + n_{22} + n_{33}) / N \quad (4)$$

$$\kappa = (p_o - p_e) / (1 - p_e) \quad (5)$$

$$F1=2PR/(P+R) \quad (6)$$

2.10 Software, data availability and ethics

All satellite data processing and modelling were conducted using Google Earth Engine for Landsat data access and preprocessing, and Python (v3.10) for machine-learning analysis, including TensorFlow (v2.15)/Keras for the CNN and scikit-learn (v 1.3.2) for the Random Forest classifier. Landsat Collection 2 Level 2 imagery is publicly available from the U.S. Geological Survey (USGS). The study used only satellite imagery and involved no human or animal subjects; therefore, ethical approval was not required.

3. RESULTS AND DISCUSSION

3.1 Spatial distribution and extent of green space

The CNN maps (**Fig. 3a–c**) reveal a consistent spatial organisation on all three dates. The peninsula's north-east and east, around the tidal creeks of the Gambia River estuary, are dominated by a large, contiguous vegetated block typical of mangrove and tidal wetland vegetation. The central and north-western peninsula is characterised by a dense built-up area and a bare core, while the south and western coastline is dominated by a mosaic of developed land and vegetation. The wetland block shows little change between dates; most of the visible changes are confined to the mosaic of the south and interior, suggesting a concentration of seasonal change in the urban fringe and fragmented vegetation. The stability of the wetland block itself is important: mangroves are one of the most carbon-rich tropical forests (Das et al., 2026; Gilang Qur'ani et al., 2024)and are located on the peninsula's closest part to the capital. This pattern is generally consistent with the national-scale mapping done by Liman Harou et al. (2023), who used Landsat and MODIS time series with a Random Forest classifier to map mangrove forests and reported a net increase of approximately 4,000 ha of mangroves along the Atlantic coast and the Gambia River over 20 years, while also indicating areas of degradation. Because single-year data cannot test such trends, the agreement concerns the presence and persistence of the wetland block and not its change. The mapping of mangroves in West Africa using Sentinel-2 and Sentinel-1 was also performed at 20 m with very high overall accuracy (95–99%), while using 30 m Landsat products in cloudy areas is inconsistent (T. Liu et al., 2021; Mondal et al., 2019), which highlights the need to use images with finer spatial resolution in future research.

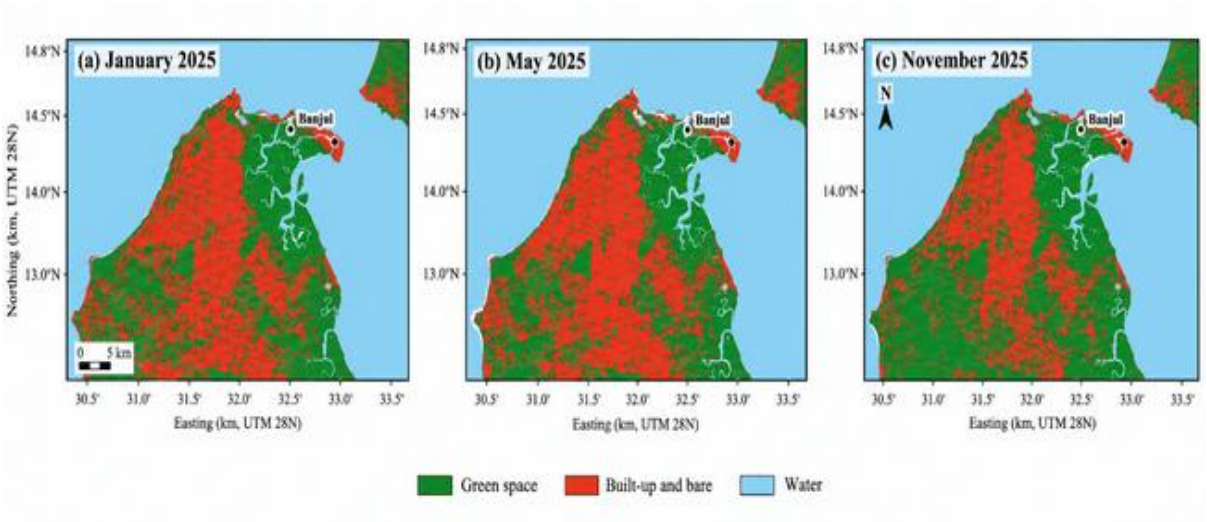


Figure 3. CNN land-cover maps of Greater Banjul for (a) January, (b) May and (c) November 2025. Masked pixels appear white.

Green space covered 20,772 ha (49.5% of land) in January, 20,588 ha (49.0%) in May, and 29,044 ha (68.0%) in November (**Table 4, Figure 4a**). The gap between January and May was just 184 ha (slightly less than 1%), while green space grew by 8,272 ha (approximately 40%) from January to November. This increment was nearly balanced by the loss of built-up and bare land (7,591 ha or approximately 36%), with the remaining change (681 ha) corresponding to the change in land area mapped between the two dates. The November gain was 100% due to areas that were not vegetated earlier in the dry season, but not due to water or masked pixels. The small change in water area (83,513 ha to 81,917 ha) could be attributed to tidal stage and cloud masking (tide state at acquisition was not controlled).

Table 4. Land-cover extent mapped by the CNN in Greater Banjul, 2025.

Class/indicator	January	May	November
Green space (ha)	20,772	20,588	29,044
Built-up and bare (ha)	21,231	21,390	13,640
Water (ha)	83,513	83,039	81,917
Land, green + built-up/bare (ha)	42,003	41,978	42,684
Green space (% of land)	49.5	49.0	68.0

Study window of 1,271 × 1,098 pixels (30 m). Pixels flagged as cloud or shadow were excluded on each date. Land totals are the sum of the two land classes.

It is important to note that the January and May shares are similar and should not be interpreted as stable vegetation cover. The classification threshold was adapted to each date's NDVI distribution; therefore, the green class is the relatively vegetated portion of the land for that date, whereas the Otsu method tends to divide a histogram into two partitions of similar sizes. Seasonal analysis revealed that the absolute vigour of the vegetation decreased significantly from January to May.

3.2 Seasonal dynamics and the consequences of threshold choice

Land NDVI decreased from a median of 0.316 in January to 0.245 in May, followed by an increase to 0.441 in November (**Figure 4b, Table 5**), representing a gain of approximately 80% from the end of the dry season to the end of the rainy season. This is because of the

distributions in Figure 4b: the May distribution is narrow with most values in the low range, whereas the November distribution is wide with values above 0.7. If the green threshold (NDVI ≥ 0.445) were used without modification for all dates, the percentage of green areas was 15.5% in January, 2.9% in May, and 49.2% in November, showing a 17-fold increase between May and November. With a fixed threshold, 97.1% of the land would qualify as non-green in May, and any date comparison would only compare phenology and not land-cover change.

This behaviour is similar to the dependency of NDVI on phenology in seasonal environments (Hussain et al., 2022; Nash et al., 2017) and (J. Liu et al., 2015) who analysed 14 Landsat 8 images over one year in southern Burkina Faso and found that most of the variation between images was due to phenology. They determined that the lowest classification accuracy was at the NDVI maximum in October, and the highest was at the NDVI minimum in a dry-season image, and that they were able to get a little better classification accuracy by placing a dry-season image with an October image. Under the fixed threshold, the green share spanned 46 percentage points across the three dates (2.9% to 49.2%), whereas the date-specific classification spans 19 percentage points (49.0% to 68.0%)

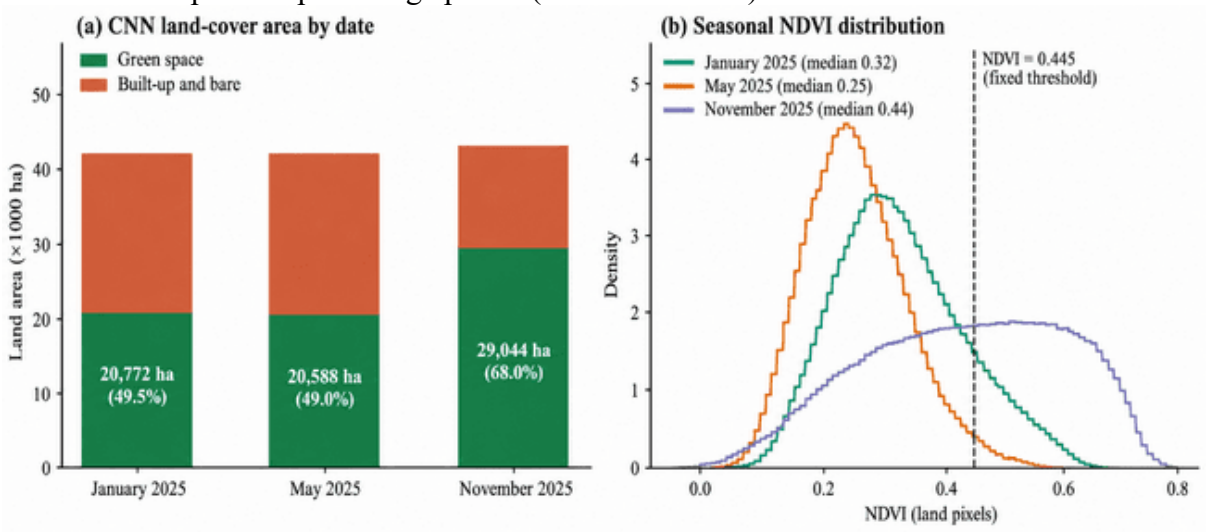


Figure 4. (a) CNN land-cover area by date and (b) distribution of land NDVI on the three dates, with a fixed threshold of 0.445.

Table 5. Seasonal vegetation signal under a fixed NDVI threshold compared with the date-specific CNN classification.

Date	Median land NDVI	Land with NDVI ≥ 0.445 (%)	CNN green space (% of land)
January 2025	0.316	15.5	49.5
May 2025	0.245	2.9	49.0
November 2025	0.441	49.2	68.0

The fixed threshold of 0.445 is the January green-class threshold. Land is defined as MNDWI < −0.05 and NDBI > −0.2. The two right-hand columns are not like-for-like: the CNN class also covers pixels in the intermediate NDVI band that were not labelled, which is consistent with the January CNN share (49.5%) exceeding the share above 0.445 (15.5%) although 0.445 is the January labelling threshold.

This result validates date-specific thresholds for within-year comparisons; however, it also provides context for the maps, as they do not reflect actual canopy cover but rather show areas where the land is relatively “green” from a seasonal perspective. The NDVI statistics describe the absolute change in vegetation throughout the seasons, and the persistence analysis below describes stable green spaces.

3.3 Persistence of green space

Persistence analysis separates stable from transient green spaces (**Figure 5, Table 6**). Of the 41,464 ha of land valid on all dates, 18,372 ha (44.3%) was green on all three dates, and 12,417 ha (29.9%) was never green. The remaining 10,675 ha (25.7%) was green on one or two dates and constitutes the seasonal component. The area green on at least one date (29,047 ha) is almost identical to the November green area (29,044 ha), so the January and May green spaces are largely contained within the November footprint. Approximately 88% of the January green space and 89% of the May green space are persistent, but only about 63% of the November green space is (these ratios are approximate, because the persistence footprint differs slightly from the date-specific land areas). Approximately 10,700 ha of the November green space is therefore seasonal.

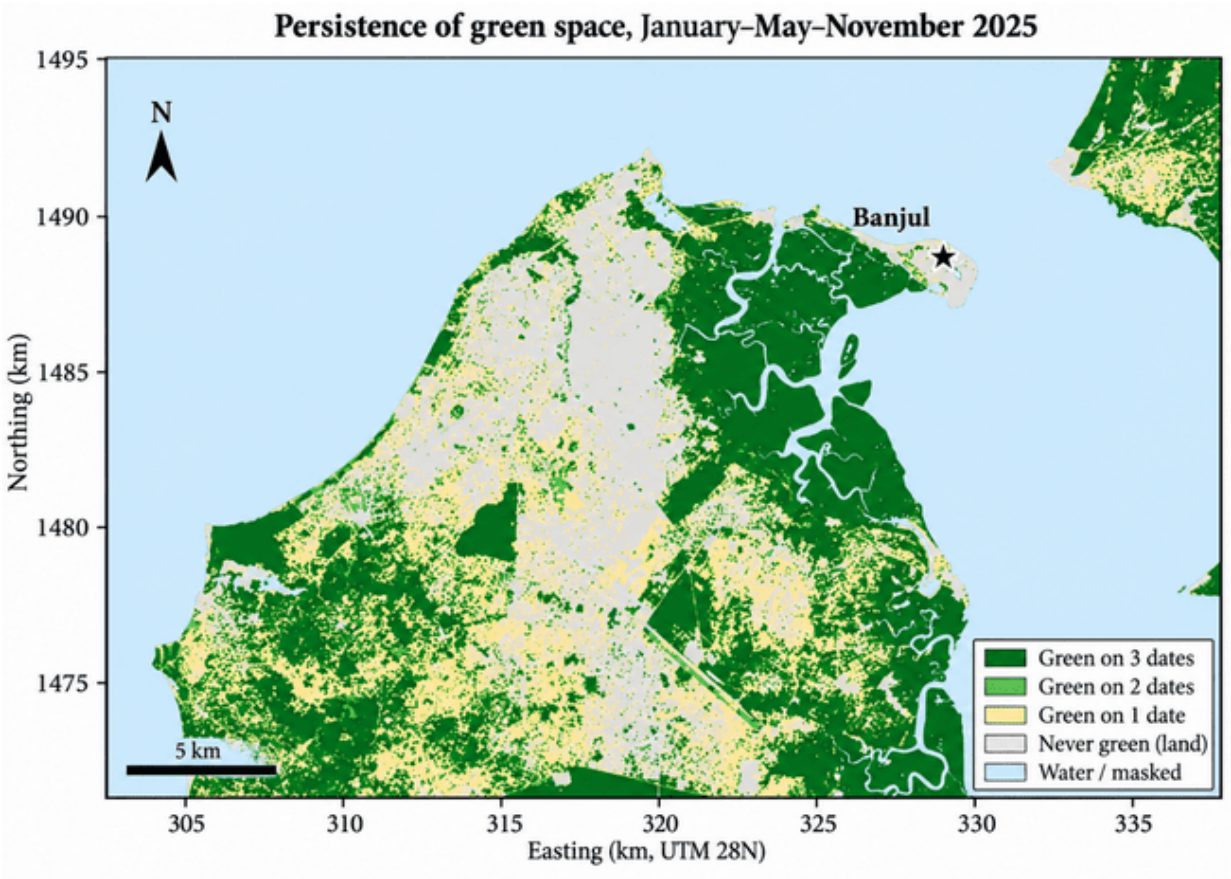


Figure 5. Persistence of green space across January, May and November 2025.

Table 6. Persistence of green space across the three image dates.

Persistence class	Area (ha)	Share of land (%)
Green on all three dates	18,372	44.3
Green on two dates	3,486	8.4
Green on one date	7,189	17.3
Never green	12,417	29.9
Total land valid on all dates	41,464	100.0

Calculated for pixels classified as land and unmasked on all three dates.

The spatial pattern (**Figure 5**) supports this interpretation. The persistent class is dominated by the eastern wetland block and several large vegetated tracts in the south, including rectilinear and elongated features that appear to correspond to institutional or airfield land. The never-green class forms the compact built-up and bare core of the peninsula. Pixels green on a single date are scattered through the south and the interior, a pattern consistent with seasonal gardens, cultivated plots, and grassland, although some will be mixed pixels at the 30 m resolution. Persistence on two or three dates is therefore the more robust indicator of stable green space. Seasonal features from an annual Landsat time series raised classification accuracy in West Sudanian savanna to 76.2%, from 68.7% and 66.1% for single dry- and rainy-season images (J. Liu et al., 2016), and in Ouagadougou, a seasonal-vegetation class, soil-like in the dry season and vegetated in the wet season, could not be mapped from single-season data (Schug et al., 2018). These studies concern accuracy and class definition and not persistence itself, but they agree with **Table 6** that a single-date map misrepresents the extent and stability of vegetation.

These findings have direct planning implications. A map from the November image alone would treat all its green space as permanent, even though approximately 37% of it is seasonal, while a dry-season map would omit the seasonal component. The 18,372-ha persistent area is the natural priority for protection, whereas the 10,675-ha seasonal component is where land-use conversion pressure and management options such as protecting urban agriculture or tree planting are most relevant. This reading agrees with evidence that cropland and garden plots in West African cities shift location and are lost as cities expand (Karg et al., 2020), with land unsuitable for construction among the factors shaping that change, and with the sharp decline in verdant land cover reported for Grand Lomé and Greater Accra under urban expansion, where forest fell from 24% to 3% and from 34% to 2% while built-up area rose from 18% to 62% and from 10% to 70% (Tossoukpe et al., 2025), which strengthens the case for securing the persistent core in Greater Banjul before conversion pressure increases.

The persistent block also matters for coastal protection, which adds to the case for giving it priority. Mangroves avert flood damages worth more than US$65 billion per year globally (Menéndez et al., 2020) A 1.0 m sea-level rise would inundate about 92 km² of The Gambia's coast, mostly wetland and mangrove (Jallow et al., 1996). These studies do not evaluate the present maps but motivate the use of the persistence map to target nature-based measures, as stable green space may persist where building is unsuitable, as in the tidal wetland.

3.4 Model behaviour and agreement with reference labels

The learning curves (**Figure 6a–c**) show that the models converged quickly, with the best validation loss reached at epoch 16 for January, 28 for May, and 15 for November, and early stopping ending training six epochs later each date. The validation loss at the selected epoch differed by orders of magnitude between dates, at about 2×10^{-5} in January, 10^{-3} in May, and 4×10^{-3} in November (read from **Figure 6a–c**), indicating that November was the most difficult date to reproduce. Training loss continued to fall after the optimum, to about 10^{-5} in January and May, and about 5×10^{-4} in November (read from **Figure 6a–c**), while validation loss levelled off or rose, a sign of mild overfitting that early stopping with weight restoration controlled. The January minimum is an isolated dip and not a stable optimum; therefore, model selection on that date is sensitive to the epoch chosen.

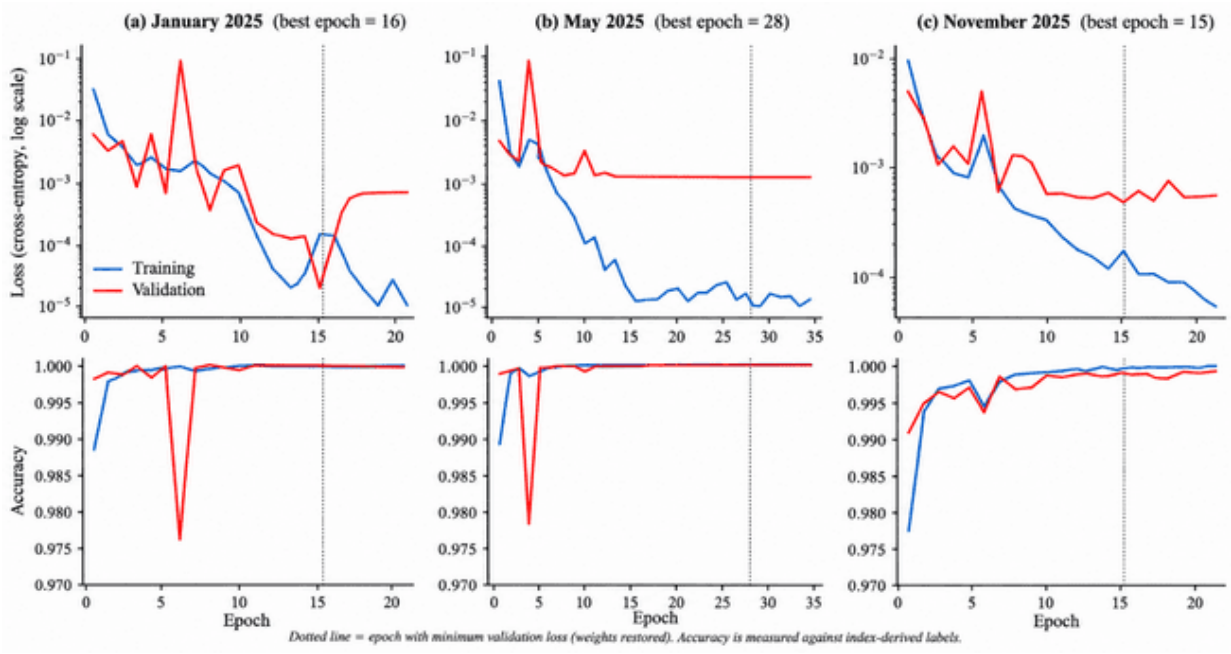


Figure 6. Training and validation loss and accuracy of the CNN for (a) January, (b) May and (c) November 2025. The dotted line marks the epoch with the minimum validation loss.

On the held-out test blocks, the CNN reached an overall accuracy of 0.9999, 0.9997, and 0.9990 and Kappa values of 0.9997, 0.9992, and 0.9979 for January, May, and November, respectively (**Table 7**). The confusion matrices (**Figure 7a–c**) show only 22, 39 and 171 misclassified pixels out of 157,685, 134,330, and 169,299, respectively. In November, 117 of the 171 errors (68%) were water pixels classified as built-up and bare land (**Figure 7c**), a confusion that is plausibly concentrated at shorelines, tidal flats, and turbid water where mixed pixels occur. The tidal phase at acquisition changes MNDWI in Landsat 8 scenes, and annual median composites are more stable than single scenes (Hickey & Radford, 2022), which makes tide state a further plausible source of this water–land confusion; tide height was not controlled.

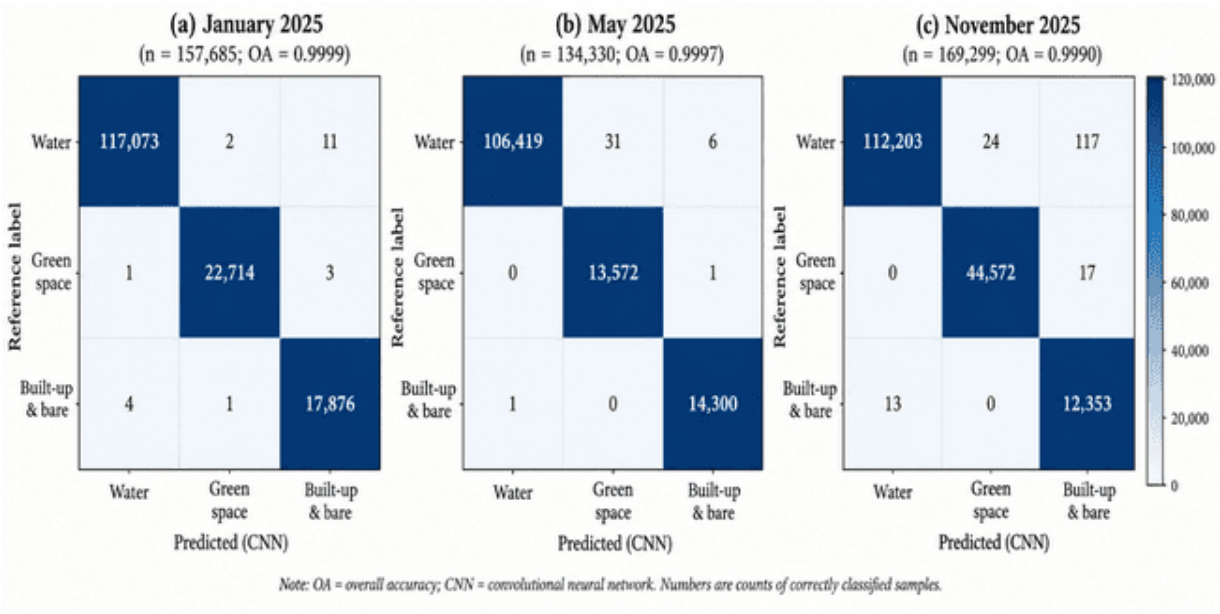


Figure 7. Confusion matrices of the CNN on the held-out test blocks for (a) January, (b) May and (c) November 2025, against index-derived reference labe

Table 7. Agreement of the CNN and Random Forest classifications with the index-derived reference labels (held-out test blocks).

Date	Model	OA	Kappa	Precision	Recall	F1-score
January	CNN	0.9999	0.9997	0.9997	0.9998	0.9997
	Random Forest	0.9997	0.9994	0.9993	0.9994	0.9993
May	CNN	0.9997	0.9992	0.9991	0.9998	0.9995
	Random Forest	0.9997	0.9992	0.9990	0.9996	0.9993
November	CNN	0.9990	0.9979	0.9962	0.9991	0.9976
	Random Forest	0.9999	0.9997	0.9995	0.9998	0.9997

OA = overall accuracy. Precision, recall and F1-score are macro-averaged over the three classes

The reference labels are deterministic threshold rules applied to the same six bands that the models receive; therefore, near-perfect scores show that both models learned the rules, as expected, and not that green space was mapped with this accuracy on the ground. The test pixels also exclude the intermediate NDVI band and are dominated by water (approximately 74%, 79%, and 66% of test pixels in January, May, and November), the easiest class; therefore, the metrics are optimistic for the vegetation boundary that matters most for green-space mapping. Agreement with labels cannot show how well the models classify the intermediate zone, which accounts for much of the land area in the CNN maps (**see the note to Table 5**). Accuracies of this order are not unusual in mangrove mapping: a U-Net applied to Landsat 8 and Sentinel-2 imagery reached 99.73% accuracy for mangroves in Myanmar (Win & Sasaki, 2024), although against different reference data, so the two values are not directly comparable. Concerns about label quality are also documented in the literature. Inconsistent or noisy training labels affect CNN performance on Landsat imagery, and spectral indices provide consistent information that can partly compensate (Zhao et al., 2022) while weak supervision is a workable route to training deep networks on Landsat imagery when pixel-level annotation is scarce (S. Wang et al., 2020), although neither study used index-rule labels. The present workflow follows this weak-supervision logic; however, as those studies imply, its outputs can be interpreted only once checked against independent reference data.

3.5 CNN compared with Random Forest

The two classifiers performed almost identically (**Table 7**). The CNN was marginally better in January (OA 0.9999 against 0.9997), the two were equal in May, and Random Forest was better in November (0.9999 against 0.9990). Differences of this size, in the third or fourth decimal place, do not support a claim that the CNN outperforms the benchmark under this evaluation. The explanation follows from the label design: when labels are threshold functions of each pixel's own bands, a per-pixel classifier is sufficient, and the CNN gains nothing from its 9 × 9 neighbourhood. Its additional spatial context could only show an advantage against labels that depend on context, such as small gardens, shaded vegetation, or bare soil adjacent to buildings. Song et al. (2019) reported a similar pattern: their patch-based light CNN for Landsat 8 land cover mapping exceeded SVM and Random Forest by less than one percentage point in overall accuracy (61.9%, 61.5% and 61.2%) and showed its clearest advantage at moderately heterogeneous pixels. Accuracy also differed by under 3% between SVM and a patch-based CNN on multitemporal Landsat 8 data (Karakizi et al., 2018), so these small margins are not unique to this study.

3.6 Limitations and future work

Five limitations qualify the findings. (i) The labels are rule-based; thus, errors in the rules propagate to the models. (ii) The date-specific thresholds make the green class relative to each date. (iii) The analysis uses one image per season in a single year; thus, inter-annual variability and the effect of rainfall anomalies are not captured. Rainfall also varies strongly between years in The Gambia; at Basse, extreme wet years clustered in 2020–2022 and extreme dry years in 2000–2002 (Jawla et al., 2026a), so a single year may not represent typical conditions. (iv) The 30 m resolution cannot resolve street trees and small gardens, which are important components of urban green space. (v) The three-class scheme does not distinguish trees, grass, crops, or mangroves, and tidal state may affect the mapping of wetland edges. Mixed pixels and training-data costs are recognised constraints on green-space mapping (Chen et al., 2021) and Landsat-based mangrove products have been inconsistent in cloudy regions (X. Liu et al., 2021), which also argues for finer-resolution data. Future work should add independent, manually interpreted training labels so that the CNN can exploit spatial context; combine Landsat with 10 m Sentinel-2 imagery (Drusch et al., 2012) and dense time series; separate vegetation types; and relate green space to population to estimate per-capita access, which would connect the maps directly to planning indicators. This direction is supported by Cardenas-Ritzert et al. (2025), who compared Sentinel-2 with very high-resolution imagery for mapping urban green and open spaces in two African cities and assessed how the choice of imagery affects SDG indicator 11.7.1.

4. CONCLUSION

This study evaluated a patch-based CNN, benchmarked against Random Forest, for mapping urban green spaces in Greater Banjul using Landsat 8 and 9 surface reflectance imagery acquired in January, May, and November 2025. Three conclusions can be drawn from these results:

The vegetation condition is strongly seasonal, and the seasonal signal is sufficiently large to dominate any given single-date map. The median land NDVI fell from 0.316 in January to 0.245 in May and rose to 0.441 in November, and a fixed NDVI threshold of 0.445 classified 15.5%, 2.9%, and 49.2% of land as green on the three dates, a seventeen-fold difference between May and November that reflects phenology and not land-cover change. Date-specific thresholds removed most of this bias; however, the resulting maps (green spaces of 49.5%, 49.0%, and 68.0% of land) show land that is comparatively green for the season and not absolute canopy cover.

The persistence analysis transformed the three dates into a usable planning product. Of the 41,464 ha of land valid on all dates, 18,372 ha (44.3%) was green on every date, 12,417 ha (29.9%) was never green, and 10,675 ha (25.7%) was green on one or two dates. The stable green space is dominated by the tidal wetland block of the north-east and east of the peninsula and by several large, vegetated tracts in the south, whereas the seasonal component lies mainly in the fragmented mosaic of the south and interior. About 37% of the November green space is seasonal; therefore, a single post-rainy map would overstate permanence, and a dry-season map would omit the seasonal component.

The CNN did not outperform the Random Forest. Agreement with the index-derived labels was near perfect for both models (CNN overall accuracy 0.9999, 0.9997, and 0.9990; Random Forest 0.9997, 0.9997, and 0.9999), with differences only in the third or fourth decimal place. Because the labels are threshold functions of each pixel's own bands, a per-pixel classifier is sufficient, and these scores show that the rules were reproduced and not that green space is mapped with this accuracy on the ground. The contribution of this study is a transparent, reproducible workflow for seasonal green-space mapping that relies only on freely

available Landsat data, and whether spatial-context learning improves accuracy remains to be settled by independent validation. The findings are also bounded by a single year with one image per season, 30 m resolution that cannot resolve street trees and small gardens, and a three-class scheme that does not separate trees, grass, crops, or mangroves.

4.1 RECOMMENDATION

Based on this, five recommendations are made:

1. For planning, the 18,372-ha persistent area, and above all the eastern tidal wetland, should be prioritised for protection in municipal and national land-use plans, while management options such as protecting urban agriculture and tree planting should be directed at the 10,675-ha seasonal component and the fragmented south, where conversion pressure is most relevant. The persistence map can also serve as a baseline for monitoring progress towards Sustainable Development Goal 11.7.
2. For monitoring, green-space maps used in planning or reporting should state their acquisition season, use date-specific or season-matched thresholds, and report persistence alongside single-date extent. The same three seasonal windows (January, May, and November) should be repeated at least annually so that land-cover change can be separated from phenology.
3. For validation, an independent stratified assessment should be completed before the maps are used for quantitative reporting, with area-adjusted accuracy and confidence intervals, and agreement with rule-based labels should not be quoted as map accuracy.
4. For methods, future work should supplement rule-based labels with manually interpreted training labels so that the CNN can exploit spatial context, add 10 m Sentinel-2 imagery and dense time series, separate vegetation types, and maintain a spatially blocked evaluation.
5. For broader application, extend the analysis to several years to capture rainfall anomalies and inter-annual variability, and link green space to population to estimate per-capita access. Because the workflow does not depend on Gambia-specific data, it can be transferred to other seasonally dry coastal cities in West Africa that face similar data constraints.

REFERENCES

Algan, G., & Ulusoy, İ. (2020). *Label Noise Types and Their Effects on Deep Learning* (Version 1). arXiv. https://doi.org/10.48550/ARXIV.2003.10471

Aram, F. (2024). Resources of Urban Green Spaces and Sustainable Development. *Resources*, *13*(1), 10. https://doi.org/10.3390/resources13010010

Bayer, A. D., Fuchs, R., Mey, R., Krause, A., Verburg, P. H., Anthoni, P., & Arneth, A. (2021). Diverging land-use projections cause large variability in their impacts on ecosystems and related indicators for ecosystem services. *Earth System Dynamics*, *12*(1), 327–351. https://doi.org/10.5194/esd-12-327-2021

Bhattad, R., Patel, V., Patel, U., & Patel, S. (2024). Implications of Batch Normalization and Dropout on Land Cover Categories in Remote Sensing. *2024 IEEE India Geoscience and Remote Sensing Symposium (InGARSS)*, 1–4. https://doi.org/10.1109/InGARSS61818.2024.10983950

Blečić, I., & Saiu, V. (2021). Assessing Urban Green Spaces Availability: A Comparison Between Planning Standards and a High-Fidelity Accessibility Evaluation. In D. La Rosa & R. Privitera (Eds.), *Innovation in Urban and Regional Planning* (Vol. 146, pp. 339–347). Springer International Publishing. https://doi.org/10.1007/978-3-030-68824-0_37

Butt, I. A., Bo, L., Butt, M. H. F., Tassew, M. T., & Bin Akhtar Khan, M. U. (2023). Enhancing Hyperspectral Image Classification: A Hybrid CNN Approach with Spatial and Channel Attention Mechanisms. *2023 20th International Computer Conference on Wavelet Active Media Technology and Information Processing (ICCWAMTIP)*, 1–5. https://doi.org/10.1109/ICCWAMTIP60502.2023.10387100

Cardenas-Ritzert, O. S. E., Shah Heydari, S., Rode, D. T., Filippelli, S. K., Laituri, M., McHale, M. R., & Vogeler, J. C. (2025). The role of data selection in mapping urban green and open spaces: A comparison across high and very-high resolution satellite imagery sources in two African cities. *Frontiers in Remote Sensing*, *6*, 1625373. https://doi.org/10.3389/frsen.2025.1625373

Carranza-García, M., García-Gutiérrez, J., & Riquelme, J. C. (2019). A Framework for Evaluating Land Use and Land Cover Classification Using Convolutional Neural Networks. *Remote Sensing*, *11*(3), 274. https://doi.org/10.3390/rs11030274

Castilla, G. (2016). We Must all Pay More Attention to Rigor in Accuracy Assessment: Additional Comment to "The Improvement of Land Cover Classification by Thermal Remote Sensing". Remote Sens. 2015, 7, 8368–8390. *Remote Sensing*, *8*(4), 288. https://doi.org/10.3390/rs8040288

Ceesay, A., Hypolite Dibi, N., Njie, E., Wolff, M., & Koné, T. (2017). Mangrove Vegetation Dynamics of the Tanbi Wetland National Park in The Gambia. *Environment and Ecology Research*, *5*(2), 145–160. https://doi.org/10.13189/eer.2017.050209

Chen, Y., Weng, Q., Tang, L., Liu, Q., Zhang, X., & Bilal, M. (2021). Automatic mapping of urban green spaces using a geospatial neural network. *GIScience & Remote Sensing*, *58*(4), 624–642. https://doi.org/10.1080/15481603.2021.1933367

Das, S., Dutta, S., Roy, J., Roy Choudhury, M., Sen, P., Chanda, A., Dutta, H., Nandi, S., & Ghosh, T. (2026). Mangroves in the Anthropocene: A global synthesis of carbon storage, biodiversity, and coastal resilience under climate and anthropogenic stressors. *Science of The Total Environment*, *1015*, 181405. https://doi.org/10.1016/j.scitotenv.2026.181405

Department of Horticulture, School of Agriculture, Lovely Professional University, India, Athokpam, V., Chamroy, T., Department of Horticulture, School of Agriculture, Lovely Professional University, India, Ngairangbam, H., & Department of Agronomy, School of Agriculture, Lovely Professional University, India. (2024). The Role of Urban Green Spaces in Mitigating Climate Change: An Integrative Review of Ecological, Social, and Health Benefits. *Environmental Reports*, *6*(1), 10–14. https://doi.org/10.51470/ER.2024.6.1.10

Drusch, M., Del Bello, U., Carlier, S., Colin, O., Fernandez, V., Gascon, F., Hoersch, B., Isola, C., Laberinti, P., Martimort, P., Meygret, A., Spoto, F., Sy, O., Marchese, F., & Bargellini, P. (2012). Sentinel-2: ESA's Optical High-Resolution Mission for GMES Operational Services. *Remote Sensing of Environment*, *120*, 25–36. https://doi.org/10.1016/j.rse.2011.11.026

Foga, S., Scaramuzza, P. L., Guo, S., Zhu, Z., Dilley, R. D., Beckmann, T., Schmidt, G. L., Dwyer, J. L., Joseph Hughes, M., & Laue, B. (2017). Cloud detection algorithm comparison and validation for operational Landsat data products. *Remote Sensing of Environment*, *194*, 379–390. https://doi.org/10.1016/j.rse.2017.03.026

García-Pardo, K. A., Moreno-Rangel, D., Domínguez-Amarillo, S., & García-Chávez, J. R. (2022). Remote sensing for the assessment of ecosystem services provided by urban vegetation: A review of the methods applied. *Urban Forestry & Urban Greening*, *74*, 127636. https://doi.org/10.1016/j.ufug.2022.127636

Gijanto, L. (2013). Historic Preservation and Development in Banjul, The Gambia. *Journal of African Diaspora Archaeology and Heritage*, *2*(1), 93–114. https://doi.org/10.1179/2161944113Z.0000000003

Gilang Qur'ani, C., Lee, B., Sasmito, S. D., Maulana, A. M., Seol, M., Wiradana, P. A., Leksono, B., Watiniasih, N. L., & Baral, H. (2024). Natural and anthropogenic impacts on mangrove carbon dynamics: A systematic review protocol. *Forest Science and Technology*, *20*(1), 1–7. https://doi.org/10.1080/21580103.2023.2272705

Güneralp, B., Lwasa, S., Masundire, H., Parnell, S., & Seto, K. C. (2017). Urbanization in Africa: Challenges and opportunities for conservation. *Environmental Research Letters*, *13*(1), 015002. https://doi.org/10.1088/1748-9326/aa94fe

Han, H., Bai, J., Ma, G., & Yan, J. (2020). Vegetation Phenological Changes in Multiple Landforms and Responses to Climate Change. *ISPRS International Journal of Geo-Information*, *9*(2), 111. https://doi.org/10.3390/ijgi9020111

Hickey, S. M., & Radford, B. (2022). Turning the Tide on Mapping Marginal Mangroves with Multi-Dimensional Space–Time Remote Sensing. *Remote Sensing*, *14*(14), 3365. https://doi.org/10.3390/rs14143365

Huang, S., Tang, L., Hupy, J. P., Wang, Y., & Shao, G. (2021). A commentary review on the use of normalized difference vegetation index (NDVI) in the era of popular remote sensing. *Journal of Forestry Research*, *32*(1), 1–6. https://doi.org/10.1007/s11676-020-01155-1

Hussain, S., Lu, L., Mubeen, M., Nasim, W., Karuppannan, S., Fahad, S., Tariq, A., Mousa, B. G., Mumtaz, F., & Aslam, M. (2022). Spatiotemporal Variation in Land Use Land Cover in the Response to Local Climate Change Using Multispectral Remote Sensing Data. *Land*, *11*(5), 595. https://doi.org/10.3390/land11050595

Isaac, E., Easwarakumar, K. S., & Isaac, J. (2017). Urban landcover classification from multispectral image data using optimized AdaBoosted random forests. *Remote Sensing Letters*, *8*(4), 350–359. https://doi.org/10.1080/2150704X.2016.1274443

J. Nhantumbo, B., A. Dada, O., & E.K. Ghomsi, F. (2023). Sea Level Rise and Climate Change – Impacts on African Coastal Systems and Cities. In Y. Zhang & Q. Cheng (Eds.), *Environmental Sciences* (Vol. 42). IntechOpen. https://doi.org/10.5772/intechopen.113083

Jallow, B., Barrow, M., & Leatherman, S. (1996). Vulnerability of the coastal zone of The Gambia to sea level rise and development of response strategies and adaptation options. *Climate Research*, *6*, 165–177. https://doi.org/10.3354/cr006165

Jawla, B., Manneh, F. J., Bah, S. A., Camara, O. M., & Danjo, S. (2026). Multi-Sensor NDVI Analysis of Eruption Impacts and Vegetation Recovery at Mount Kelud, East Java (2013–2025). *Jurnal Sains Geografi*, *4*(1), 1–23. https://doi.org/10.21009/JSG.v4i1.01

Jawla, B., Manneh, F. J., & Hardianto, Y. Z. M. Y. (2026). Spatiotemporal Assessment of Landslide-Induced Vegetation Dynamics Using Landsat Satellite Imagery (NDVI), Mount Rinjani, Indonesia (2018-2026). *Journal of Environmental Protection*, *17*(05), 342–364. https://doi.org/10.4236/jep.2026.175016

Jawla, B., Manneh, F. J., Bah, S. A., Camara, O. M., Danjo, S., & Trawally, M. L. (2026). Assessment of solar resource availability and its climatic drivers at a representative grid point in The Gambia. *Journal of Marine-Earth Science Technology, 6*(3), 134–150. https://doi.org/10.12962/j27745449.v6i3.10582

Jawla, B., Manneh, F. J., Bah, S. A., Camara, O. M., & Danjo, S. (2026). Rainfall and wind variability in Basse, The Gambia: Temporal trends, extreme events, and inter-variable relationships (2000–2025). *Journal of Marine-Earth Science Technology, 6*(3), 117–133. https://doi.org/10.12962/j27745449.v6i3.9904

Ji, L., Zhang, L., Wylie, B. K., & Rover, J. (2011). On the terminology of the spectral vegetation index (NIR − SWIR)/(NIR + SWIR). *International Journal of Remote Sensing*, *32*(21), 6901–6909. https://doi.org/10.1080/01431161.2010.510811

K. Harsha, V. R., & D. Gowri, S. R. (2022). Analysis of modified water index (MWI) for extraction of water bodies in Landsat-8 imagery. *I-Manager's Journal on Image Processing*, *9*(1), 18. https://doi.org/10.26634/jip.9.1.18526

Karakizi, C., Karantzalos, K., Vakalopoulou, M., & Antoniou, G. (2018). Detailed Land Cover Mapping from Multitemporal Landsat-8 Data of Different Cloud Cover. *Remote Sensing*, *10*(8), 1214. https://doi.org/10.3390/rs10081214

Karg, H., Drechsel, P., Dittrich, N., & Cauchois, A. (2020). Spatial and temporal dynamics of croplands in expanding West African cities. *Urban Agriculture & Regional Food Systems*, *5*(1), e20005. https://doi.org/10.1002/uar2.20005

Khalil, R., Khan, M. S., Hasan, Y., Nacer, N., & Khan, S. (2024). Supervised NDVI Composite Thresholding for Arid Region Vegetation Mapping. *Engineering, Technology & Applied Science Research*, *14*(3), 14420–14427. https://doi.org/10.48084/etasr.7202

Kulkarni, A. D. (2025). Multispectral Image Analysis Using Deep Neural Networks. *International Journal of Advanced Computer Science and Applications*, *16*(9). https://doi.org/10.14569/IJACSA.2025.0160902

Li, J., Khodadadzadeh, M., Plaza, A., Jia, X., & Bioucas-Dias, J. M. (2016). A Discontinuity Preserving Relaxation Scheme for Spectral–Spatial Hyperspectral Image Classification. *IEEE Journal of Selected Topics in Applied Earth Observations and Remote Sensing*, *9*(2), 625–639. https://doi.org/10.1109/JSTARS.2015.2470129

Liman Harou, I., Inyele, J., Minang, P., & Duguma, L. (2023). Understanding the states and dynamics of mangrove forests in land cover transitions of The Gambia using a Fourier transformation of Landsat and MODIS time series in Google Earth Engine. *Frontiers in Forests and Global Change*, *5*, 934019. https://doi.org/10.3389/ffgc.2022.934019

Liu, J., Heiskanen, J., Aynekulu, E., Maeda, E., & Pellikka, P. (2016). Land Cover Characterization in West Sudanian Savannas Using Seasonal Features from Annual Landsat Time Series. *Remote Sensing*, *8*(5), 365. https://doi.org/10.3390/rs8050365

Liu, J., Heiskanen, J., Aynekulu, E., & Pellikka, P. K. E. (2015). Seasonal variation of land cover classification accuracy of Landsat 8 images in Burkina Faso. *The International Archives of the Photogrammetry, Remote Sensing and Spatial Information Sciences*, *XL-7/W3*, 455–460. https://doi.org/10.5194/isprsarchives-XL-7-W3-455-2015

Liu, T., Lawluvy, Y., Shi, Y., & Yap, P.-S. (2021). Low Impact Development (LID) Practices: A Review on Recent Developments, Challenges and Prospects. *Water, Air, & Soil Pollution*, *232*(9), 344. https://doi.org/10.1007/s11270-021-05262-5

Liu, X., Fatoyinbo, T. E., Thomas, N. M., Guan, W. W., Zhan, Y., Mondal, P., Lagomasino, D., Simard, M., Trettin, C. C., Deo, R., & Barenblitt, A. (2021). Large-Scale High-Resolution Coastal Mangrove Forests Mapping Across West Africa With Machine Learning Ensemble and Satellite Big Data. *Frontiers in Earth Science*, *8*, 560933. https://doi.org/10.3389/feart.2020.560933

Menéndez, P., Losada, I. J., Torres-Ortega, S., Narayan, S., & Beck, M. W. (2020). The Global Flood Protection Benefits of Mangroves. *Scientific Reports*, *10*(1), 4404. https://doi.org/10.1038/s41598-020-61136-6

Mondal, P., Liu, X., Fatoyinbo, T. E., & Lagomasino, D. (2019). Evaluating Combinations of Sentinel-2 Data and Machine-Learning Algorithms for Mangrove Mapping in West Africa. *Remote Sensing*, *11*(24), 2928. https://doi.org/10.3390/rs11242928

Nash, M., Wickham, J., Christensen, J., & Wade, T. (2017). Changes in Landscape Greenness and Climatic Factors over 25 Years (1989–2013) in the USA. *Remote Sensing*, *9*(3), 295. https://doi.org/10.3390/rs9030295

Neyns, R., & Canters, F. (2022). Mapping of Urban Vegetation with High-Resolution Remote Sensing: A Review. *Remote Sensing*, *14*(4), 1031. https://doi.org/10.3390/rs14041031

Ngandam Mfondoum, A. H., Gbetkom, P. G., Cooper, R., Hakdaoui, S., & Mansour Badamassi, M. B. (2020). EXTRACTING BUILT-UP FEATURES IN COMPLEX BIOPHYSICAL ENVIRONMENTS BY USING A LANDSAT BANDS RATIO. *The International Archives of the Photogrammetry, Remote Sensing and Spatial Information Sciences*, *XLIV-M-2–2020*, 79–85. https://doi.org/10.5194/isprs-archives-XLIV-M-2-2020-79-2020

Otsu, N. (1979). A Threshold Selection Method from Gray-Level Histograms. *IEEE Transactions on Systems, Man, and Cybernetics*, *9*(1), 62–66. https://doi.org/10.1109/TSMC.1979.4310076

Papaiordanidis, S., Minakou, C., & Gitas, I. Z. (2020, December 2). ON-THE-FLY LAND COVER MAPPING USING MACHINE LEARNING WITH MULTISPECTRAL SATELLITE IMAGERY ON GOOGLE EARTH ENGINE. *Лесные Экосистемы в Условиях Изменения Климата: Биологическая Продуктивность и Дистанционный Мониторинг*. Лесные экосистемы в условиях изменения климата: биологическая продуктивность и дистанционный мониторинг. https://doi.org/10.25686/7229.2020.6.58827

Ploton, P., Mortier, F., Réjou-Méchain, M., Barbier, N., Picard, N., Rossi, V., Dormann, C., Cornu, G., Viennois, G., Bayol, N., Lyapustin, A., Gourlet-Fleury, S., & Pélissier, R. (2020). Spatial validation reveals poor predictive performance of large-scale ecological mapping models. *Nature Communications*, *11*(1), 4540. https://doi.org/10.1038/s41467-020-18321-y

Pozhar, V. E. (2025). Spectral Indices. Determination and Interpretation Problems. *2025 Wave Electronics and Its Application in Information and Telecommunication Systems (WECONF)*, 1–4. https://doi.org/10.1109/WECONF65186.2025.11017157

Proutsos, N. D., & Solomou, A. D. (2025). Urban Green Spaces as an Effective Tool to Regulate Urban Climate and Biodiversity: Current Research and Challenges. *Land*, *14*(3), 497. https://doi.org/10.3390/land14030497

Qian, Y., Zhou, W., Pickett, S. T. A., Yu, W., Xiong, D., Wang, W., & Jing, C. (2020). Integrating structure and function: Mapping the hierarchical spatial heterogeneity of urban landscapes. *Ecological Processes*, *9*(1), 59. https://doi.org/10.1186/s13717-020-00266-1

Ridwana, R., Danoedoro, P., Herumurti, S., Himayah, S., Ihsan, M., Arrasyid, R., & Urfan, F. (2019). Linear Spectral Mixture Analysis Land Cover for Assessment Level Subpixel: A Case Study of Tasikmalaya City Area Based on Landsat Imagery. *IOP Conference Series: Earth and Environmental Science*, *286*(1), 012042. https://doi.org/10.1088/1755-1315/286/1/012042

Roberts, D. R., Bahn, V., Ciuti, S., Boyce, M. S., Elith, J., Guillera-Arroita, G., Hauenstein, S., Lahoz-Monfort, J. J., Schröder, B., Thuiller, W., Warton, D. I., Wintle, B. A., Hartig, F., & Dormann, C. F. (2017). Cross-validation strategies for data with temporal, spatial, hierarchical, or phylogenetic structure. *Ecography*, *40*(8), 913–929. https://doi.org/10.1111/ecog.02881

Sanampreet. (2020). URBAN GREEN SPACES: THEIR IMPORTANCE IN ENVIRONMENTAL CONSERVATION. In Dr. Jagdish Kumar Sahu, Ms. Sruthi S, Arun Adwani, (Dr.) T Ch Anil Kumar, & Mr. Nikhil Bhagat, Mr. Sourabh Batar, *INTERSECTING REALMS: NEW DIMENSIONS IN MULTIDISCIPLINARY RESEARCH, VOLUME-2* (1st ed.). RED UNICORN PUBLISHING. https://doi.org/10.25215/9358091800.38

Sasikala, B. S., Biju, V. G., & Prashanth, C. M. (2017). Kappa and accuracy evaluations of machine learning classifiers. *2017 2nd IEEE International Conference on Recent Trends in Electronics, Information & Communication Technology (RTEICT)*, 20–23. https://doi.org/10.1109/RTEICT.2017.8256551

Schug, F., Okujeni, A., Hauer, J., Hostert, P., Nielsen, J. Ø., & Van Der Linden, S. (2018). Mapping patterns of urban development in Ouagadougou, Burkina Faso, using machine learning regression modeling with bi-seasonal Landsat time series. *Remote Sensing of Environment*, *210*, 217–228. https://doi.org/10.1016/j.rse.2018.03.022

Semeraro, T., Scarano, A., Buccolieri, R., Santino, A., & Aarrevaara, E. (2021). Planning of Urban Green Spaces: An Ecological Perspective on Human Benefits. *Land*, *10*(2), 105. https://doi.org/10.3390/land10020105

Song, H., Kim, Y., & Kim, Y. (2019). A Patch-Based Light Convolutional Neural Network for Land-Cover Mapping Using Landsat-8 Images. *Remote Sensing*, *11*(2), 114. https://doi.org/10.3390/rs11020114

Tossoukpe, A. Y., Dukiya, J., Folega, F., Thiel, M., & Okhimamhe, A. A. (2025). Dynamics of Changes in Spatial Patterns of Built-Up Areas in Two Metropolitan Areas of Grand Lomé and Greater Accra (West Africa). *Urban Science*, *9*(3), 84. https://doi.org/10.3390/urbansci9030084

Tucker, C. J. (1979). Red and photographic infrared linear combinations for monitoring vegetation. *Remote Sensing of Environment*, *8*(2), 127–150. https://doi.org/10.1016/0034-4257(79)90013-0

United Nations Department of Economic and Social Affairs. (2019). *World Urbanization Prospects: The 2018 Revision*. UN. https://doi.org/10.18356/b9e995fe-en

Waldner, F. (2020). The T Index: Measuring the Reliability of Accuracy Estimates Obtained from Non-Probability Samples. *Remote Sensing*, *12*(15), 2483. https://doi.org/10.3390/rs12152483

Wang, S., Chen, W., Xie, S. M., Azzari, G., & Lobell, D. B. (2020). Weakly Supervised Deep Learning for Segmentation of Remote Sensing Imagery. *Remote Sensing*, *12*(2), 207. https://doi.org/10.3390/rs12020207

Wang, Y. (2024). Strategic Planning of Urban Green Space at Large Spatiotemporal Scales. *Forests*, *15*(6), 1022. https://doi.org/10.3390/f15061022

Webb, J. L. A. (1992). ECOLOGICAL AND ECONOMIC CHANGE ALONG THE MIDDLE REACHES OF THE GAMBIA RIVER, 1945–1985. *African Affairs*, *91*(365), 543–565. https://doi.org/10.1093/oxfordjournals.afraf.a098561

Wei, X., Xu, M., Zhao, H., Liu, X., Guo, Z., Li, X., & Zha, T. (2024). Exploring Sensitivity of Phenology to Seasonal Climate Differences in Temperate Grasslands of China Based on Normalized Difference Vegetation Index. *Land*, *13*(3), 399. https://doi.org/10.3390/land13030399

Win, K., & Sasaki, J. (2024). The Change Detection of Mangrove Forests Using Deep Learning with Medium-Resolution Satellite Imagery: A Case Study of Wunbaik Mangrove Forest in Myanmar. *Remote Sensing*, *16*(21), 4077. https://doi.org/10.3390/rs16214077

Wulder, M. A., Loveland, T. R., Roy, D. P., Crawford, C. J., Masek, J. G., Woodcock, C. E., Allen, R. G., Anderson, M. C., Belward, A. S., Cohen, W. B., Dwyer, J., Erb, A., Gao, F., Griffiths, P., Helder, D., Hermosilla, T., Hipple, J. D., Hostert, P., Hughes, M. J., … Zhu, Z. (2019). Current status of Landsat program, science, and applications. *Remote Sensing of Environment*, *225*, 127–147. https://doi.org/10.1016/j.rse.2019.02.015

Wulder, M. A., Roy, D. P., Radeloff, V. C., Loveland, T. R., Anderson, M. C., Johnson, D. M., Healey, S., Zhu, Z., Scambos, T. A., Pahlevan, N., Hansen, M., Gorelick, N., Crawford, C. J., Masek, J. G., Hermosilla, T., White, J. C., Belward, A. S., Schaaf, C., Woodcock,

C. E., … Cook, B. D. (2022). Fifty years of Landsat science and impacts. *Remote Sensing of Environment*, *280*, 113195. https://doi.org/10.1016/j.rse.2022.113195

Xie, D., Depoian, A. C., Jaques, L. E., & Bailey, C. P. (2021). A convolutional fully connected structure with hard sample memory pool for land use classification. In M. S. Alam (Ed.), *Pattern Recognition and Tracking XXXII* (p. 12). SPIE. https://doi.org/10.1117/12.2588025

Xu, H. (2006). Modification of normalised difference water index (NDWI) to enhance open water features in remotely sensed imagery. *International Journal of Remote Sensing*, *27*(14), 3025–3033. https://doi.org/10.1080/01431160600589179

Yao, J., Feng, W., Yang, L., Ju, L., Li, X., & Zhao, X. (2022). Multi-scale fully convolutional network-based land cover classification method for remote sensing images. In S. Zhu, Q. Yu, J. Su, L. Chen, & J. Chu (Eds.), *Eighth Symposium on Novel Photoelectronic Detection Technology and Applications* (p. 271). SPIE. https://doi.org/10.1117/12.2624366

Zaznov, I., Badii, A., Kunkel, J., & Dufour, A. (2025). AdamZ: An enhanced optimisation method for neural network training. *Neural Computing and Applications*, *37*(32), 26887–26914. https://doi.org/10.1007/s00521-025-11649-w

Zeng, Y., Jia, L., Menenti, M., Jiang, M., Barnieh, B. A., Bennour, A., & Lv, Y. (2023). Changes in vegetation greenness related to climatic and non-climatic factors in the Sudano-Sahelian region. *Regional Environmental Change*, *23*(3), 92. https://doi.org/10.1007/s10113-023-02084-5

Zha, Y., Gao, J., & Ni, S. (2003). Use of normalized difference built-up index in automatically mapping urban areas from TM imagery. *International Journal of Remote Sensing*, *24*(3), 583–594. https://doi.org/10.1080/01431160304987

Zhang, M., & Hong, L. (2018). Deep Learning Integrated with Multiscale Pixel and Object Features for Hyperspectral Image Classification. *2018 10th IAPR Workshop on Pattern Recognition in Remote Sensing (PRRS)*, 1–8. https://doi.org/10.1109/PRRS.2018.8486304

Zhao, X., Wu, J., Wang, H., Gao, X., & Zhao, L. (2022). Injecting spectral indices to transferable convolutional neural network under imbalanced and noisy labels for Landsat image classification. *International Journal of Digital Earth*, *15*(1), 437–462. https://doi.org/10.1080/17538947.2022.2036833f